On Generation and Analysis of Synthetic Finger-Vein Images for Biometrics Identification

Fieke Hillerström, Ajay Kumar
Department of Computing
The Hong Kong Polytechnic University
Email: csfhhillerstrom@comp.polyu.edu.hk, csajaykr@comp.polyu.edu.hk

Abstract: The finger-vein biometric offers a higher degree of security, personal privacy and strong anti-spoofing capabilities than most other biometric modalities employed today. Emerging privacy concerns with the database acquisition and lack of availability of large scale finger-vein databases have posed challenges in exploring this technology for large scale applications. This technical report details the *first* such attempt to synthesize finger-vein images and presents analysis of synthesized images for the biometrics authentication. We generate a database of 50,000 finger-vein images, corresponding to 5000 different subjects, with 10 different synthesized finger-vein images from each of the subject. We use tractable probability models to compare synthesized finger-vein images with the *real* finger-vein images for their image variability. This report also presents matching accuracy of a biometric recognition algorithm, using the synthesized finger-vein database from 5000 different subjects, using 225,000 genuine and 1249,750,000 impostor matching scores, which suggests significant promises from this finger-vein biometric modality for large scale biometrics applications. This research also developed a user-friendly software to synthesize finger-vein image databases, which could help to advance further research in finger-vein biometrics.

1. Introduction

Biometric identification using finger-vein patterns typically matches the profile of subcutaneous finger-vein network. The finger-vein biometric is not visible with naked eye under normal illumination conditions, which makes it very difficult to covertly acquire and extremely difficult to alter their integrity. Therefore finger-vein biometrics offers high degree of privacy, anonymity, security and anti-spoofing capability over other popular biometrics like face, iris or even fingerprint. Several databases of finger-vein images have recently been introduced [KZ12, YLS11, TV13, ZLL+13, MASR14]. However, these databases are relatively smaller than those available for face or iris and involve a small number of subjects for imaging (see table 2). Therefore it is impossible to undertake the developed identification algorithms to extensive testing. The acquisition of large scale biometric databases is expensive and inconvenient for the subjects and comes with the privacy concerns related with biometrics. In order to address some of these problems, several synthetic biometric databases have been developed [Cap04, ZSC07, WHST08]. However, finger-vein image synthesis had not yet attained the attention of researchers.

In this technical report we develop a finger-vein image synthesis model, based on vein pattern growth from nodes to patterns, which incorporates realistic imaging variations to synthesize finger-vein images for biometrics. The anatomy of the finger-veins is firstly analyzed (section 3) and the influence of finger-vein acquisition methods is then introduced (section 4). These formulations are used as a basis for the generation of synthetic finger-vein images (section 5). The performance of a developed synthetic finger-vein image database is analyzed (section 6), using tractable probability models and also the actual matching performance.

2. Related Prior Work

There has been an increasing interest to explore vascular patterns for biometrics identification [KP09], [KZ12]. Several commercial systems have already been introduced and available for commercial usage. Earlier efforts to match finger-vein patterns using repeated line tracking approach is described in [MNM04]. Yang *et al*. [YSY10] investigated the finger-vein authentication using a bank of Gabor filters. Several publications illustrate local binary pattern based matching of finger-vein features [RSS11, LLP09]. One of the most comprehensive works on finger-vein identification, with comparison of multiple finger-vein matchers on relatively larger database, appears in [KZ12]. This report also proposes to enhance finger-vein identification using simultaneously extracted fingerprint images.

Another approach to improve finger-vein recognition accuracy is to perform restoration of finger-vein images degraded by the light scattering in the finger skin. Such an approach is described in [YSY12] and uses a biologically motivated optical model. Lee and Park [LP11] use an image restoration model that can account for optical blur and skin scattering, to improve the finger-vein matching accuracy.

Table 1: Summary of prior work on biometric image synthesis for different modalities.

Modality	**Ref.**	**Approach**	**Database**
Iris	[ZSC07]	Generation of synthetic fibers and adding top layers	200 individuals, 2 iris classes per individual, 6 iris images per class
Fingerprint	[Cap04]	Generation of directional map and ridge pattern, combined with a density map	Adjustable up to 100000 fingers with each up to 100 samples
Face	[BV99]	Forming linear combinations of prototypes derived from real faces	Not provided
Palmprint	[WHST08]	Patch-based sampling on extracted principle lines	300 classes with each 20 images. Total images: 6000
Finger-Vein	*This Report*	Random vein pattern growth combined with imaging variability models	**5000** subjects with each 10 finger-vein images, Total images: **50,000**

Table 2: Summary of the finger-vein image databases developed in the references.

Database	**Ref.**	**Size**	**Sessions**	**Public**
Hong Kong Polytechnic University	[KZ12]	6264 images from 156 subjects, 2 fingers per subject	2	Yes
SDUMLA-HMT	[YLS11]	3816 images, 6 fingers per subjects	1	Yes
University of Twente	[TV13]	1440 images of 60 subjects	2	No
FV-USM	[MASR14]	5904 images of 123 subjects, 492 different finger classes	2	Yes
CFVD	[ZLL+13]	1345 images of 13 subjects, 130 different fingers	2	No

Synthesis of biometric images enables modeling of vital anatomical evidences underlying the respective biometric images and noise obscuring the recovery of underlying features. The image synthesis also enables development of large scale biometrics databases for the performance evaluation and improvement in the real systems. Another use of synthesized biometrics database lies in detecting and evaluating integrity of a given biometrics system. There have been several promising efforts to synthesize biometrics image databases for other popular biometric modalities. Table 1 summarizes such related prior work and also underlines our work in this report.

3. Anatomy of Finger-Veins

The veins in the fingers can be divided into two sets, the superficial veins and the deep veins. The deep veins lay usually alongside the arteries, where the superficial veins are closer to the surface of the body [Gra18]. The superficial veins of the hand contain the dorsal digital veins and the palmar digital veins, which pass along the sides of the fingers and contain a venous network in between [Gra18] (see figure 1). Loda states that the veins in the finger are located almost exclusively at the dorsal side of the finger [Lod99]. From the nail, small veins meet at the distal interphalangeal joint where they form one or two small central veins, with a diameter of

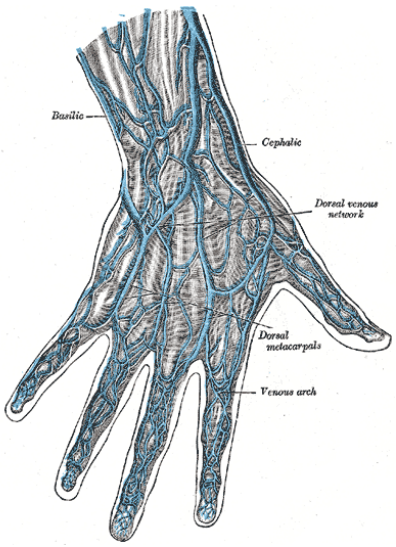

Figure 1: The veins on dorsum of the hand [Gray18].

approximately 0.5 mm [Lod99]. The veins become more prominent and numerous at the proximal interphalangeal level, where they form anastomotic arches. Sukop *et al.* [SND+07] found that the three-phalanx fingers contain the same typical statistics about the dorsal venous systems (figure 2). There are two veins at both the radial and ulnar side of the proximal phalanx with a diameter over 1 mm, leading to the hand palm. These two veins form an arch above the proximal phalanx [SND+07] (see figure 3 and 4).

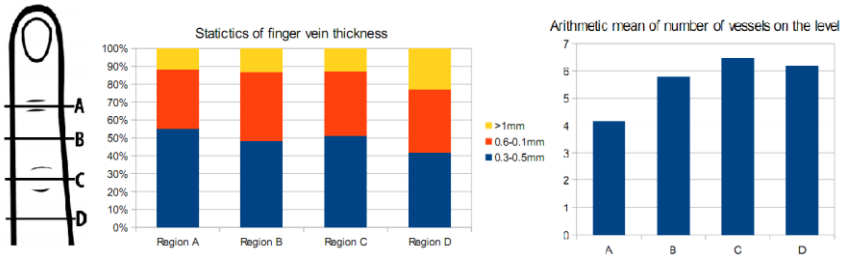

Figure 2: Typical statistics of blood veins in human fingers.

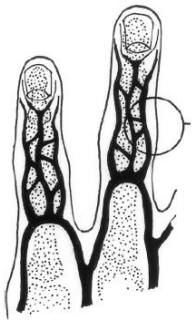

Figure 3: Two veins form an arch above the proximal phalanx [SND+07].

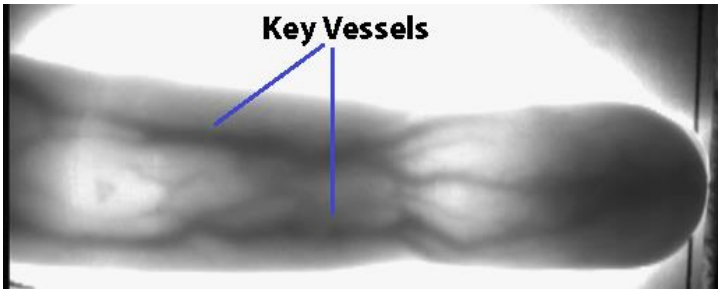

Figure 4: Indication of the two key veins in a real finger-vein image from [KZ12].

4. Imaging Variation in Finger-Vein Images

The finger-vein imaging typically uses near infrared (NIR) spectroscopy, with a wavelength between 700nm to 1400nm [XS08]. The veins become visible, because of the hemoglobin in the blood plasma. At 760 nm light-absorption is almost only performed by de-oxidized hemoglobin and not by oxidized hemoglobin (see figure 5) [CC+07]. When a suitable wavelength is chosen, the arteries, which contain mostly HbO, will not be visible in the finger-vein image. The NIR-scanning device cannot penetrate deep into the skin and therefore the deep veins

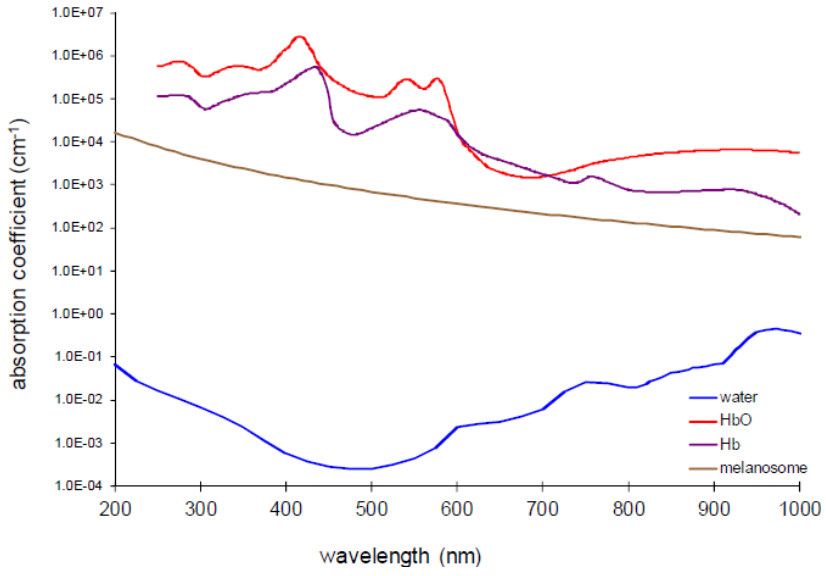

Figure 5: Absorption coefficient of water, oxyhemoglobin, deoxyhemoglobin and melanin for different wavelengths [Cup12]

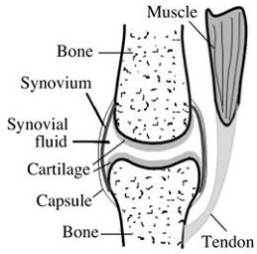

Figure 6: Anatomy of an interphalangeal joint [YS12]

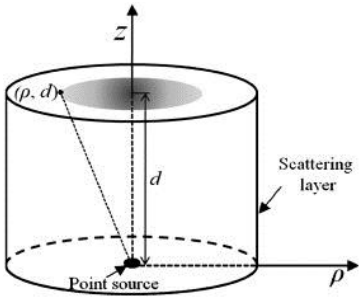

Figure 7: Visual interpretation of the scattering blur from the point sources.

are not captured in the images [CC+07]. The interphalangeal joints result in a higher light penetration through the finger, because the joint is filled with fluid, which has a lower density than bones (see figure 6) [YS12]. This is the key reason for the illumination variation commonly observed in finger-vein images.

The NIR-illumination from the source is absorbed by the human tissues, which mainly consists of the skin, bones and vessels. The transmitted light (I_{tr}) after attenuation can be estimated as follows:

$$I_{tr} = I_0 e^{-\mu D} \quad (1)$$

where I_0 represents the finger-vein image without any degradation, D is the depth of the object and μ is the transport attenuation coefficient [YSY12].

While acquiring the finger-vein patterns, the images are expected to be degraded, due to scattering and optical blur. Such depth-of-field blur of the camera can be modeled using Gaussian blur [KP07], whose parameters can be experimentally estimated. Such point spread function (PSF) can be defined as

$$h(x,y) = \frac{1}{2\pi\sigma^2} e^{-\frac{x^2+y^2}{2\sigma^2}} \quad (2)$$

with as parameters $\sigma = kR$ and (x,y) are the spatial indices. k is a parameter determined by the camera properties. R represents the radius of the blur, defined as;
$R = \frac{Ds}{2}(\frac{1}{f} - \frac{1}{u} - \frac{1}{s})$ in which D is the diameter of the lens aperture, s the distance between the lens and the image plain, f the focal distance of the camera and u the distance between the lens and the object, which will vary for every finger-vein image.

The finger-vein images are also expected to be degraded due to skin scattering, which can be modeled by a model which includes the absorption and scattering coefficients of the skin and the thickness of the skin [LP11]. At a wavelength of 850 nm the absorption and scattering coefficients of the finger skin are 0.005 and 0.61 mm^{-1} respectively and that the thickness of the finger skin is about 3-4 mm [LP11]. The PSF can be defined as

$$P_s(\rho) = \frac{3P_I}{(4\pi)^2}\left((\mu_s' + \mu_a) + \left(\kappa_d + \frac{1}{\sqrt{\rho^2+d^2}}\right)\frac{d}{\sqrt{\rho^2+d^2}}\right) * \frac{e^{-\kappa_d\sqrt{\rho^2+d^2}}}{\sqrt{\rho^2+d^2}} \quad (3)$$

with P_I the total power of illumination at a point in the vein region, d the depth of a point from the skin surface, ρ the distance perpendicular to the direction of d (see figure 7). κ is defined as $\kappa_d = 3\mu_a(\mu_s' + \mu_a)$. μ_a is the absorption coefficient of the skin and μ_s' the reduced scattering coefficient.

These three PSFs describe the often observed image variations in finger-vein images. often degrade the quality of finger-vein images. (1) can be used to model the NIR-light transmission through the human finger, after which (2) and (3) can be used to model the often observed image degradation due to blur.

5. Synthesizing Finger-Vein Images

The proposed method for generating synthetic finger-vein images can be divided into three main parts (see figure 8). Firstly the root vein nodes are generated, based on several node parameters. The root vein nodes are sample points of a vein pattern, which in a later step are grown to a vein pattern. These root vein nodes are different for different fingers, but are assumed to be stable for images from the same finger, since they represent the anatomy of the finger. The root vein nodes are used to grow the thickened vein patterns for the synthesized image. Finally the grown vein patterns are used to transform into acquired finger-vein images by incorporating the absorption and scattering of skin and blood (see figure 9). Each of these three key steps is described in the following three subsections.

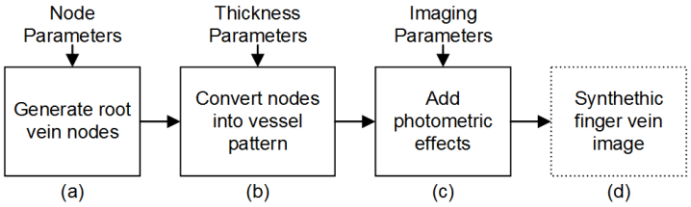

Figure 8: Block diagram of key steps for synthesizing finger vein images

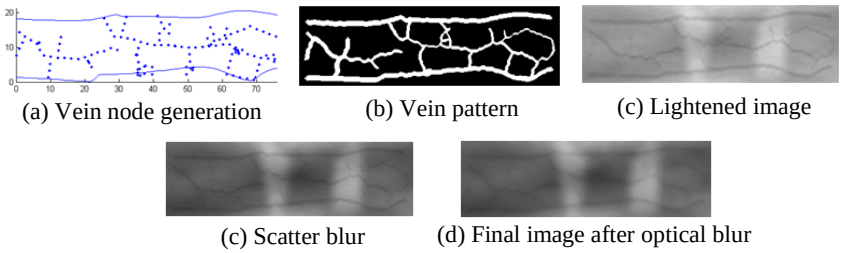

(a) Vein node generation (b) Vein pattern (c) Lightened image

(c) Scatter blur (d) Final image after optical blur

Figure 9: Typical output corresponding to key steps of Figure 8

5.1 Vein Node Generation

The root finger-vein nodes, which can be seen as sample points of the vein pattern, are generated, using a *grow* method, inspired by the generation of leaf venation patterns proposed in reference [RFL+05]. This model makes use of sources, which influence the direction in which new vessel nodes will be *grown*. An iterative loop is used, to *grow* the veins towards the sources, until the algorithm has converged (see figure 10 & 11). During this iterative process new sources are added, which should be further than a *birth distance* B_d from the other sources and veins. A source is removed when a vein reaches that source in the *kill distance* K_d.

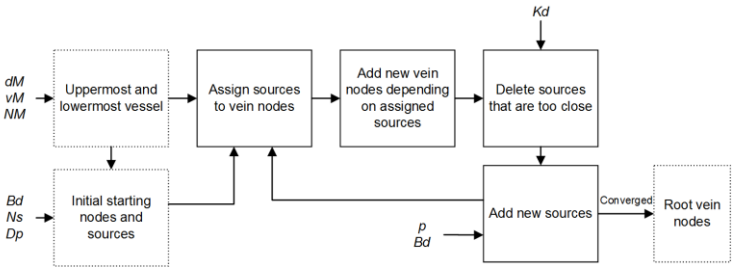


```
Generate vein nodes
initialize sources, starting point
while(~Converged)
    for  P = every active point
        S = find all sources that are relative neighbor
        if(dist(Si,P) < Dk && source not linked to other node)
            remove Si
        end
        if(size(S) > 0)
            V = normalize(sum(normalize(Si – P)))
            Pnew = P + V
        end
    end
    if(size(Sstable) > 0)
        Snew = new random source, dist(all P, Snew) > Bd
    end
end
```

Figure 10: Block diagram and the pseudocode of the key steps for the vein node generation.

The generation of vein nodes largely depends on the sources in the neighborhood. Sources are linked to vein nodes, if they are relative neighbors of each other. Two points are relative neighbors from each other if they are at least as close to each other as they are to any other point [Tou08]. For every source linked to a vein node, the normalized vector between them is calculated and these vectors are added up. A new vein node is grown in the resulting direction of this vector. Two vein nodes growing to the same source are very unlikely to reach that source at the same time. Therefore the source should be remained until all nodes growing to the source are in the killing distance of that source.

In our approach the generation of vein nodes begins with two[1] key vessels, on which some stable sources are chosen. Around and between these main vessels, random sources are placed. There are two types of sources, *stable sources* and *random sources*. The stable sources are placed on the main vessels, in order to create a mesh in between them. The random sources are placed randomly between and around the main vessels and influence the way in which the veins grow towards the stable sources. The new placed sources during the iterations are random sources. Because the algorithm resulted in single line endings too often, the endings of line elements are added as sources for other line elements, if they are close enough to each other.

The growing of new vein nodes will continue until all sources are deleted, or until the sources do not result in new nodes anymore. After all the stable sources are removed, no more new sources will be placed. The finger is divided in three parts based on the locations of the phalanges and according to the statistics observed in [BK10]. Depending on the different part of the finger, the statistics of the source placement differs (see table 3). We select randomly located starting points, to begin the vein generation process.

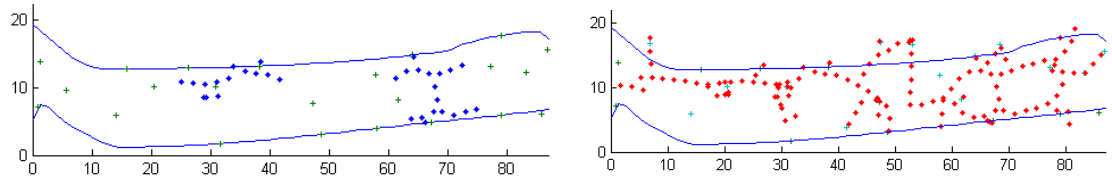

Figure 11: Visualisation of the vein node generation. (* vein nodes, + sources)

[1] At least two, as indicated from anatomical studies in [SND+07].

Table 3: Details on the parameters used to model the root vein nodes.

Parameter	**Values**
Length of the proximal phalanx	39.78 ± 4.94 mm [BK10]
Length of the medial phalanx	22.38 ± 2.51 mm [BK10]
Length of the distal phalanx	15.82 ± 2.26 mm [BK10]
Soft tissues of tip of distal phalanx	3.84 ± 0.59 mm [BK10]
Distance between source and vein node, in which source will be removed (*Kd)*	Uniform between 1 and 2
Distance needed for generating a new source in the proximal phalanx *(Bdp)*	Uniform between 4 and 7
Distance needed for generating a new source in the middle phalanx *(Bdm)*	Uniform between 4 and 6
Distance needed for generating a new source in the distal phalanx *(Bdd)*	Uniform between 4 and 5
Distance needed for generating a new source at the edges of the finger *(Bde)*	Uniform between 2 and 5
Distance needed between the starting points *(Bds)*	Uniform between 3 and 10
Distance for which endpoints of lines are added as sources of other vein nodes	Uniform between 5 and 12
Density of generated sources in distal phalanx *(Dpd)*	Uniform between $\frac{1}{200}$ and $\frac{1}{130}$
Density of generated sources in middle phalanx *(Dpm)*	Uniform between $\frac{1}{210}$ and $\frac{1}{135}$
Density of generated sources in proximal phalanx *(Dpp)*	Uniform between $\frac{1}{220}$ and $\frac{1}{140}$
Amount of stable sources in proximal phalanx *(Nsp)*	3 - 5
Amount of stable sources in middle phalanx *(Nsm)*	3 – 5
Amount of stable sources in top phalanx *(Nst)*	2 - 3
Amount of stable sources on the edges of the finger *(Nse)*	2 - 3
Amount of starting vein nodes *(Nss)*	2 – 3
Change that a new source point is generated *(p)*	Uniform between 0.3 and 0.5
Stepsize between two new nodes	2
Finger width	20 mm
Average distance from main vessels from edge *(dM)*	Uniform between 1.5 and 5.5
Variance in distance from main vessel from edge *(vM)*	Uniform between 1 and 2
Amount of sample points for main vessel generation *(NM)*	4 – 8
Distance for source placing outside main vessels	3

In order to reduce the computational requirements, we incorporate active vein nodes in our model. When a vein node was not linked to any of the sources for two times, the node becomes inactive. Inactive nodes will not be processed anymore. When a new source is added, all the vein nodes in a certain distance are made active again, to make it possible to grow new nodes towards those newly placed sources.

5.2 Vein Pattern Generation

Once the desired vein nodes have been generated, these nodes are connected into a thickened pattern that characterizes a vascular network (see figure 12). For every image from the same subject and same finger, a small distortion is added to the positions of the vein nodes, by randomly shifting the basic vein pixels a few pixels. The main vein points and the other vein points are connected to each other separately, using dilation and thinning.

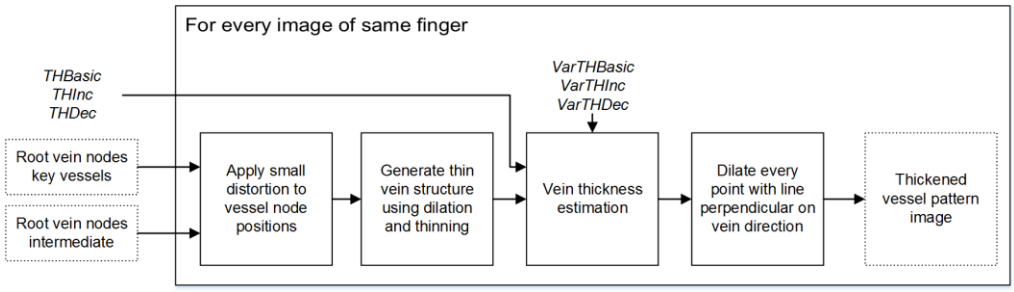

Figure 12: Block diagram of the key steps used to convert the vein nodes into a vein pattern

The thickness of the veins is computed, using random basic parameters with small fluctuations for genuine or intra-class images (see table 4). The key uppermost and lowermost vessels are firstly thickened and this process starts from the top (nail end) of the fingers. For every vessel point a small amount of thickness is added. The branches are processed, starting with the veins that branches out of the key vessels (see figure 13). Reference [RFL+05] use Murray's law to calculate the thickness of the branched leaf veins, using $r_{parent}^3 = \sum_1^n r_{child_n}^3$, where r_{parent} represents the thickness of the vein before branching and r_{child} is the thickness of the veins that branches out of the parent vein. This step is incorporated likewise, with the simplification that every child gets the same thickness, $r_{child}^3 = \frac{r_{parent}^3}{N_{child}}$. For every new vein point, the thickness is decreased by small amount/pixels. Veins that are between two branchpoints of a different thickness are assigned the average thickness of both branchpoints. After the thickness is computed for every vein point, the thinned vein pattern is converted into a thicken image using dilation with a perpendicular line onto the vein direction.

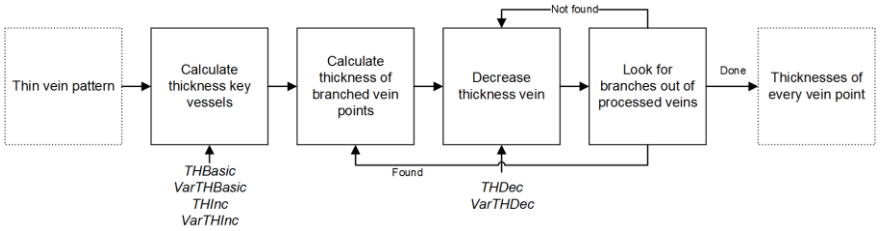


```
Compute basic thickness veins
find right key vessel ends

while(~ end key vessel)
    thickness node =  THBasic + THInc + VarTHInc
end
while(~Done)
    B = find branches
    THBranch = sqrt3(THparent^3/length(B))
    for every B
        THnode = THBranch
        while(~(End branch || New branch))
            THnextNode = THNode – THDec - VarTHDec
        end
    end
end
```

Figure 13: Block diagram and the pseudocode of the key steps for the vein thickness estimation of Figure 12

Table 4: Details on the parameters used for the conversion into vessel patterns.

For generating images of different subjects	
Parameter	*Values*
Width of the dilation structure	15
Minimum thickness of the main vessel *(THBasic)*	Uniform between 7.5 and 9.4
Thickness increasing for main vessel *(THInc)*	Uniform between 0.006 and 0.01 – THBasic / 2000
Thickness decreasing for branches *(THDec)*	Uniform between 0.001 and 0.002 * THBasic
For generating images of same subjects	
Parameter	*Values*
Variation in minimum thickness of main vessel *(VarTHBasic)*	Uniform between -2 and 2
Variation in increasing factor for images of same subjects *(VarTHInc)*	Uniform between -0.006 and 0.006
Variation in decreasing factor for images of same subjects *(VarTHDec)*	Uniform between -0.0005 and 0.0005 * THBasic /2
Variation in the place of the vessel nodes	4
Variation in the place of the nodes of the main vessels	2

5.3 Finger-Vein Image Generation

The expected influence due to the illumination and the imaging setup are incorporated in the vein pattern images generated (figure 14) from previous section (figure 12). The basic vein patterns generated from the steps in figure 14 are firstly band pass filtered using a Gabor filter, to accentuate different part of the vein patterns. The filter is used for one orientation, with a small variation for every different image of the same subject. The 10 percent lowest outcome values of the Gabor filtering, will be attenuated by a predefined factor (fixed as 4 in our experiments). The illumination effects and variations are modeled using equations (1), (2) and (3). The effect of the depth of the tissues in the finger is varied for every subject and this variation is kept smaller for intra-class images.

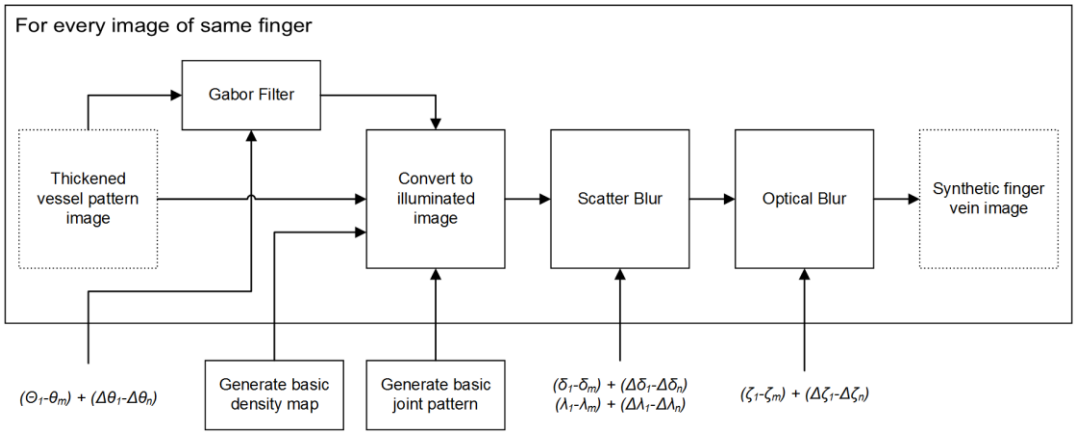

Figure 14: The block diagram for the key steps in the process employed to convert the vein *patterns* into finger-vein images corresponding to near-infrared imaging in the developed synthetic database.

The bones of the fingers are modeled, using an elliptic function and have a thickness of about 1 cm. The interphalangeal joints are mimicked as two regions of 1.5 - 2 cm, in which the bone thickness is expected to be smaller, according to the observations made in [YS12]. Random points are generated in these areas, which are dilated and the convex hull of these dilated points is estimated. This convex hull is used as area to mimic the interphalangeal joint. For every image generated from the same subject this joint area is marginally adjusted, using the dilation and erosion with different structuring elements.

In order to incorporate the overall near-infrared illumination (back-lightening) and variability in this illumination from the interphalangeal joints areas, Perlin noise is used. Perlin noise can be used to create coherent noise over space [Per]. Perlin noise with large variety is used to create a more skin like structure and Perlin noise with low variety mimics the overall changes in the light transmission. The parameters incorporated in our synthesis model are provided in table 5.

5.4 Graphical User Interface

In order to make the synthetic finger-vein image database generation more convenient for the users, a graphical user interface (GUI) has been developed. During the startup of the GUI, the default values are loaded, which can be adjusted thereafter. The GUI can be used for two purposes: to visualize the influence of the parameter values and to generate a synthetic finger-vein database, based on the chosen parameters. When choosing the visualization, the generated vein nodes, the finger-vein pattern and the final finger-vein image, generated based on the lower values of the specified parameters, will be shown for one sample. This mode is the mode in which the GUI is started, after which it first displays default images.

When the '*Generate database'* box is checked, a synthetic finger-vein database will be generated for the amount of subjects and images specified. The location in which the database will be saved, must be specified in order to start the generation. The images will be saved in that location in a folder '*GeneratedImages*' and the images for every subject will be saved in a separate folder. The images are saved in the '.tiff' format which preserves all the information. The GUI will close automatically after the complete generation of database.

The '*Generate*' button will start the generation of the sample images or the generation of the database. Using the '*Reset*' button, the default values will be loaded again. The layout of the graphical user interface is shown in figure 15.

Table 5: Details on the parameters used for the modeling of synthetic finger-vein images

Generating images from different subjects	
Parameter	*Values*
Skin thickness	Uniform between 1.5 and 3.5 mm
Range of the basic density map	Values between 0.72 and 1.32
Factor in which bone thickness at joints decreases	Between 0.805 and 0.986
Light absorption of the vessels	40 * skinThickness
Light absorption of skin used in lightening image	200
Light absorption of bones used in lightening image	30
Basic orientation of the Gabor filter (θ_1 - θ_m)	Uniform between $\frac{\pi}{5}$ and $\frac{4\pi}{5}$
Frequency of the Gabor filter	0.08
Size of the Gabor filter	19
Basic depth of the vessels (δ_1 - δ_m)	Uniform between 7 and 15 mm
Basic depth of the tissue (λ_1 - λ_m)	Uniform between 3 and 5 mm
Absorption coefficient of skin used in scatter blur	0.005 / mm
Scattering coefficient of skin used in scatter blur	0.61 / mm
Camera parameter *k* for optical blur	$\frac{1}{7}\sqrt{3}$
Distance between lens and image plane (ζ_1 - ζ_m)	3.06524 mm
Diameter of lens aperture	6 mm
Basic distance between lens and finger	Uniform between 4 and 6 mm
Focal length of camera	2.753 mm
Width of the joint regions	Uniform between 1.5 and 2 mm
Generating images from same subjects	
Parameter	*Values*
Dilation and erosion width for adjusting joint regions	Uniform between 8 and 10
Dilation and erosion structures	Diamond, disk or square
Range of Perlin noise to adjust the joint regions	Between 0.7 and 1.3
Variation of orientation of Gabor filter ($\Delta\theta_1$ - $\Delta\theta_n$)	Uniform between -0.1 and 0.1
Multiplication factor of the basic density map	Uniform between 0.99 and 1.01
Variation in the depth of the vessels ($\Delta\delta_1$ - $\Delta\delta_n$)	Uniform between -3 and 3
Variation in the depth of the tissues ($\Delta\lambda_1$ - $\Delta\lambda_n$)	Uniform between -0.25 and 0.25
Variation in the distance between lens and finger ($\Delta\zeta_1$ - $\Delta\zeta_n$)	Uniform between -0.5 and 0.5 mm
Thickness of the vessels	Uniform between 2 and 3 mm

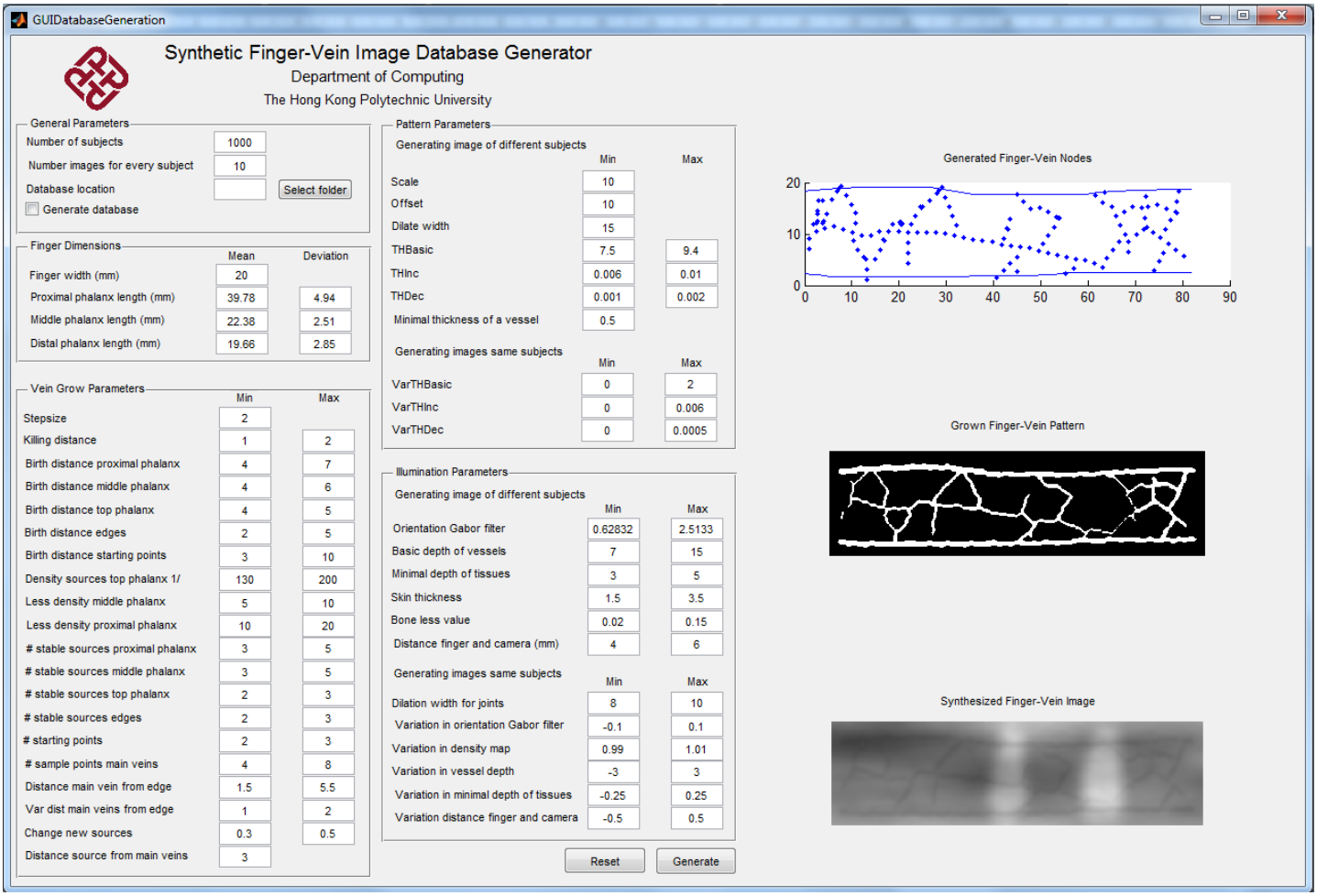

Figure 15: Layout of the graphical user interface for synthetic finger-vein image database generation

6. Experiments and Results

6.1 Database Generation

We evaluated the proposed approach to synthesize the finger-vein images by generating a large database of 50,000 finger-vein images corresponding to 5000 different subjects. Some of the sample images from the proposed approach are reproduced in figure 16. This figure also includes image samples from the real finger-vein database acquired in [KZ12]. It can be ascertained from the visual inspection that the quality of synthesized finger-vein images is quite similar to those acquired from the real finger-vein imaging setup. The images in figure 17 illustrates typical intra-class and inter-class variations in the synthesized finger-vein images. The images in figure 18, 19, 20 and 21 show the possible extremities in the synthetic finger-vein image generation, for this generated database.

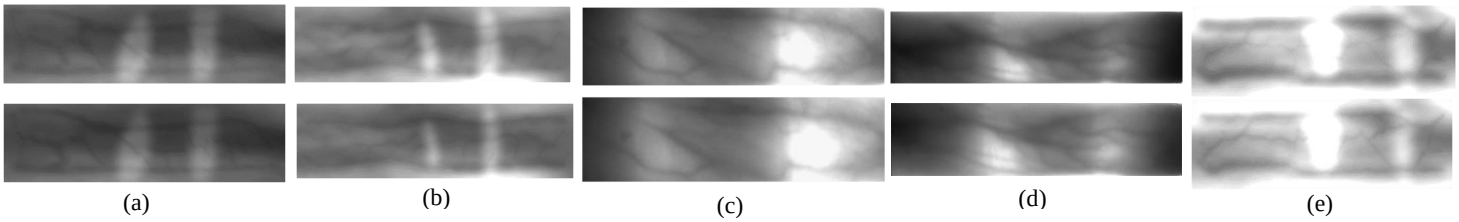

(a) (b) (c) (d) (e)

Figure 16: Sample images from the synthesized finger-vein databse in (a), (b) and (e). The images in (c) & (d) are real images from database in [KZ12]

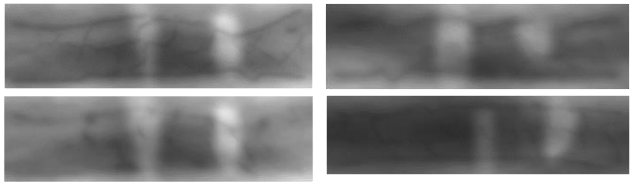

(a) Intra-Class (Same Subject) (b) Inter-Class (Different Subject)

Figure 17: Sample images to illustrate inter-class similarity and intra-class variability

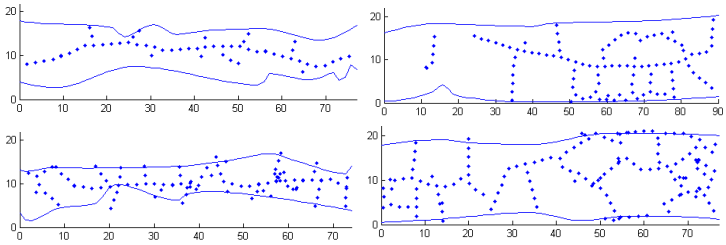

Figure 18: Extremeties in the vein node generation

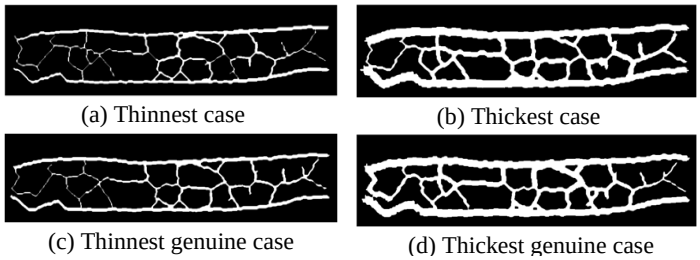

(a) Thinnest case (b) Thickest case

(c) Thinnest genuine case (d) Thickest genuine case

Figure 19: Extremeties in the thickness of the vein patterns

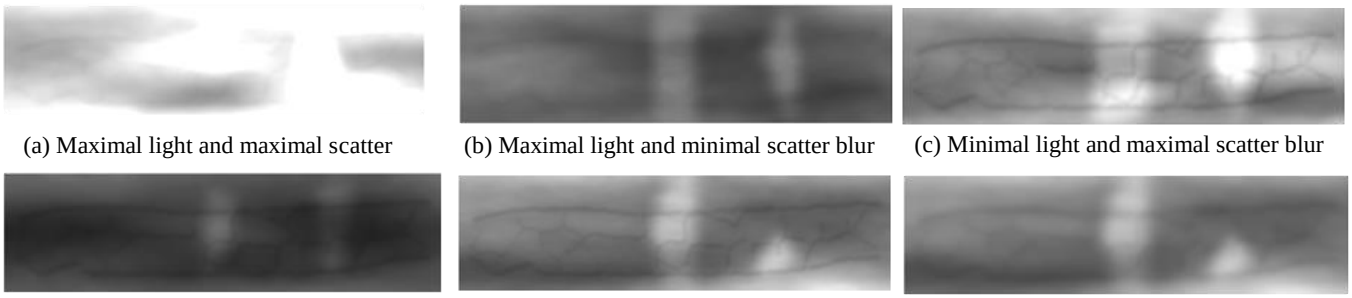

(a) Maximal light and maximal scatter (b) Maximal light and minimal scatter blur (c) Minimal light and maximal scatter blur

(d) Minimal light and minimal scatter blur (e) Minimal optical blur (f) Maximal optical blur

Figure 20: Extremities in the illumination (Inter-Class)

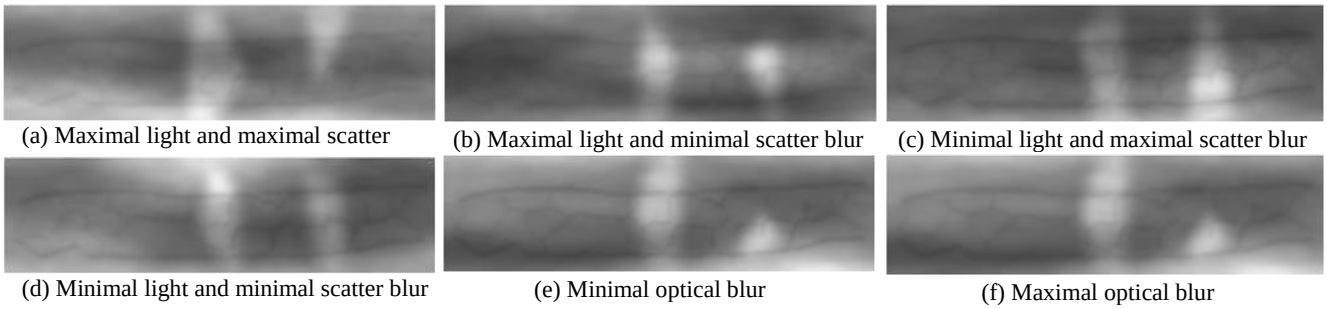

(a) Maximal light and maximal scatter (b) Maximal light and minimal scatter blur (c) Minimal light and maximal scatter blur

(d) Minimal light and minimal scatter blur (e) Minimal optical blur (f) Maximal optical blur

Figure 21: Extremities in the illumination (Intra-Class)

6.2 Similarity Analysis between Synthesized and Real Images

In order to ascertain distinguishability of synthesized vein images with those acquired from real imaging setup, we model their lower-order probability densities of pixel values in the respective images using Bessel K form [GS01, Sri02]. It is based on a weighted superposition of 2D object profiles at given Poisson points: $I(z) = \sum_{i=1}^{n} a_i g_i(z - z_i)$, with z_i the Poisson points, g_i randomly chosen object profiles and a_i a weigth factor, uniform between 0 and 1 [Sri02]. Grenander and Srivastava [GS01] show that these Bessel K forms can be represented by two parameters: a shape parameter p, $p > 0$ and a scale parameter c, $c > 0$. The image level comparison can be performed by comparing the Bessel K forms of two (filtered) images.

Given an image I and a filter F, the filtered image I_i can be recovered by $I_i = I*F$, where * denotes a 2D convolution. Under the conditions as stated in [Sri02], the density functions of the filtered image I_i can be approximated by

$$f(x; p, c) = \frac{1}{Z(p, c)} |x|^{p-0.5} K_{(p-0.5)}\left(\sqrt{\frac{2}{c}}|x|\right) \qquad (4)$$

where K the modified Bessel function and Z a normalization constant, given by

$$Z(p,c) = \sqrt{\pi}\Gamma(p)(2c)^{0.5p+0.25} \quad (5)$$

In order to estimate the required probability density functions, the parameters p and c have to be determined, based on the observed image pixel data, using

$$\hat{p} = \frac{3}{SK(I_i)-3} \text{ and } \hat{c} = \frac{SV(I_i)}{\hat{p}} \quad (6)$$

where SK represents the sample kurtosis and SV represents sample variance of the pixel values in I_i. Since the estimation of p is sensitive to the outliers, the estimation is replaced by an estimation based on quantiles, as proposed in [ZSC07]:

$$\widehat{SK}(I_i) = \frac{q_{0.995}(I_i) - q_{0.005}(I_i)}{q_{0.75}(I_i) - q_{0.25}(I_i)} \quad (7)$$

where $q_x(.)$ is the quantile function, that returns the x quantile of a set of samples. In order to analyze the performance on texture level, three images are selected: a synthetic finger-vein image, a real finger-vein image and a natural image. The images are scaled to the same size and the intensity values scaled to the same level. Thereafter a difference image between the original image and a 5 horizontal pixels shifted version is computed and Gabor filtered. Their estimated and observed pixel densities are comparatively illustrated figure 22. We selected 8 images from each of the three groups (real, synthetic, natural) and estimated their parameters as shown in table 6. The range of the estimated parameters from the real finger-vein images is quite similar or close to those from the synthesized finger-vein images. However these parameters are significantly different with those from the natural images.

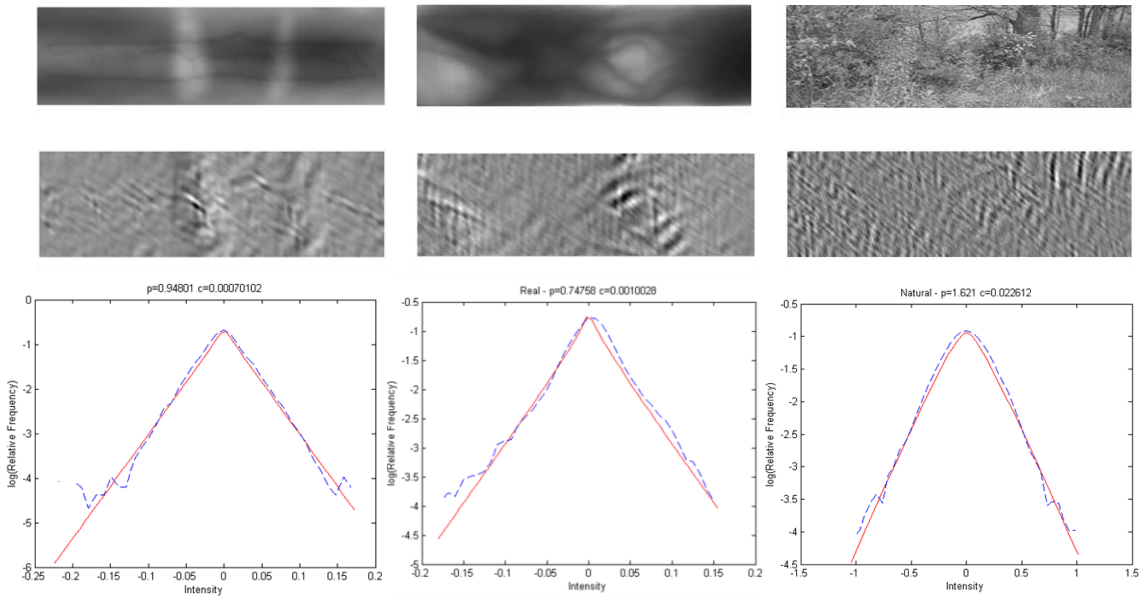

(a) Synthetic (b) Real (c) Natural

Figure 22: Original images, their filtered versions and their observed densities (dashed lines) and estimaed Bessel K forms

Table 6: Estimated Bessel K parameters for different images

Synthetic		**Real**		**Natural**	
p	c	p	c	p	c
1.10	$5.85\ 10^{-4}$	1.13	$4.36\ 10^{-4}$	3.86	0.062
0.81	$4.67\ 10^{-4}$	1.21	$5.85\ 10^{-4}$	0.60	0.11
1.03	$5.56\ 10^{-4}$	1.73	$1.49\ 10^{-4}$	1.62	0.023
1.04	$5.01\ 10^{-4}$	0.75	0.0010	1.21	0.026
1.30	$4.58\ 10^{-4}$	1.12	$4.51\ 10^{-4}$	0.94	0.021
1.27	$3.69\ 10^{-4}$	1.49	$7.01\ 10^{-4}$	1.02	0.031
0.90	$4.13\ 10^{-4}$	1.32	0.0017	1.32	0.024
1.08	$5.00\ 10^{-4}$	1.25	$6.44\ 10^{-4}$	2.14	0.22

In order to determine the differences between two Bessel K forms, different distance measures can be explored. The KL divergence [Sri02] between two density functions f_1 and f_2 is defined as follows:

$$d_{KL}(f_1||f_2) = \int_{IR} \log\left(\frac{f_1(x)}{f_2(x)}\right) f_1(x)dx \quad (8)$$

The L^2-metric [Sri02] between two Bessel K can be computed as follows:

$$d_I = \sqrt{\int_x \left(f(x;p_1,c_1) - f(x;p_2,c_2)\right)^2 dx} \quad (9)$$

Using these distance measures, the Bessel K forms for the twelve images, four selected from each groups, *i.e.*, real, synthetic and natural, are compared and classified. All images were scaled/selected to be of same size where after the difference image is computed and Gabor filtered. Their Bessel K forms are estimated and compared, using the both distance measures in equation (8) and (9). The dendrogram plots in figure 23 illustrate the results of the classifications, based on these comparisons. In this figure, number 1-4 denote natural images, 5-8 denotes real finger-vein images and 9-12 denote synthetic finger-vein images. It can be observed that the natural images are distinctly classified from the finger-vein images in both the cases.

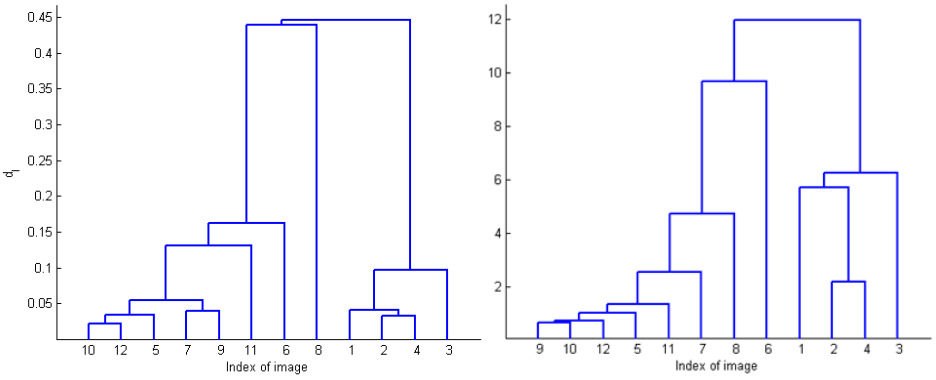

Figure 23: Dendrogram clustering of the distance metrics d_I (left) and d_{KL} (right). 1-4 natural, 5-8 real finger vein, while 9-12 are synthetic finger-vein images

6.3 Identification Performance

The key purpose of synthetic finger-vein generation is for the performance evaluation of biometric recognition algorithms. The recovery of finger-vein images using anatomical characteristics and incorporating realistic imaging variations, such as from the model in this report, can help to estimate upper bound [KK13] on the performance from the finger-vein matching technologies. We ascertain finger-vein matching performance from the database corresponding to 5000 subjects using their 50,000 synthesized finger-vein images. The matcher employed in our experiments is based on recovering and matching binary pattern (LBP). The synthetic images are firstly enhanced, using the histogram equalization. The normalized LBP histograms are then computed, using 8 subparts, a radius of 5 pixels and 8 sample points on this radius. The matching scores are computed from the histogram similarity using the Chi squared distance [Gag10]. We generated 225,000 genuine scores and 1249,750,000 impostor scores to estimate the matching accuracy for large scale database. The normalized histogram of these scores is shown in figure 24, while its receiver operating characteristics is shown in figure 25. The experiments achieve an equal error rate of 1.63%.

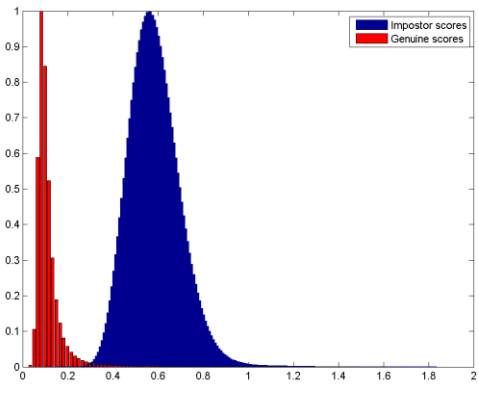

Figure 24: Normalized histograms of the genuine and impostor scores (5000 subjects)

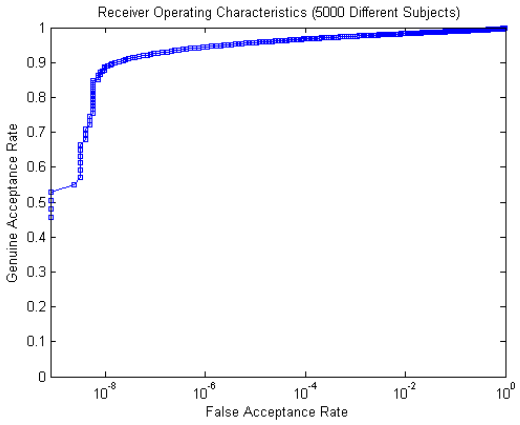

Figure 25: Receiver operating characteristics from synthetic finger vein images (5000 subjects)

This low equal error rate implies achieved from matching large (synthetic) finger-vein images illustrate significant discriminant capability of finger-vein biometrics, *i.e.*, low intra-class variations from the basic vascular structure and large inter-class separation in matching scores. We also generated another set of synthetic finger-vein image database but with different values for the lightening parameters (see table 7). The objective was to ascertain effect of parameter variations in the distribution of inter- and intra-class matching scores from the synthetic finger vein images generator developed in this work. This database corresponds to 750 subjects with 7500 synthesized finger-vein images. Again LBP classification and the Chi squared distance is used to generate 33750 genuine scores and 28,087,500 impostor scores. The normalized histogram of these scores is

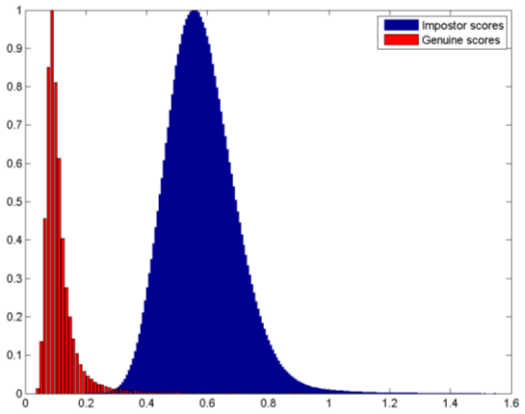

Figure 26: Normalized histograms of the genuine and impostor scores (750 subjects)

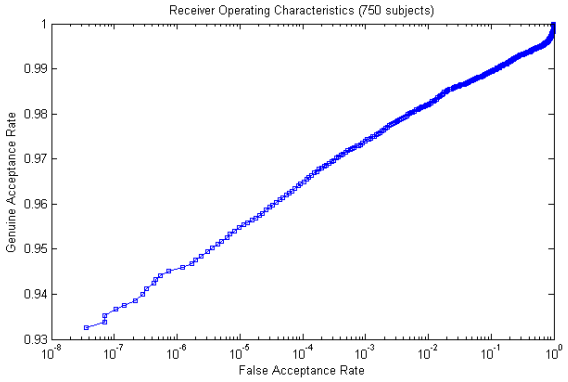

Figure 27: Receiver operating characteristics from synthetic finger vein images (750 subjects)

Table 7: Details on the parameters used for the modeling of synthetic finger-vein images (750 subjects)

Generating images from different subjects	
Parameter	*Values*
Skin thickness	Uniform between 1.5 and 3.5 mm
Range of the basic density map	Values between 0.35 and 0.72
Factor in which bone thickness at joints decreases	Between 0.805 and 0.986
Light absorption of the vessels	40 * skinThickness
Light absorption of skin used in lightening image	200
Light absorption of bones used in lightening image	30
Basic orientation of the Gabor filter (θ_1 - θ_m)	Uniform between $\frac{\pi}{5}$ and $\frac{4\pi}{5}$
Frequency of the Gabor filter	0.08
Size of the Gabor filter	19
Basic depth of the vessels (δ_1 - δ_m)	Uniform between 7 and 15 mm
Basic depth of the tissue (λ_1 - λ_m)	Uniform between 3 and 5 mm
Absorption coefficient of skin used in scatter blur	0.005 / mm
Scattering coefficient of skin used in scatter blur	0.61 / mm
Camera parameter *k* for optical blur	$\frac{1}{7}\sqrt{3}$
Distance between lens and image plane (ζ_1 - ζ_m)	3.06524 mm
Diameter of lens aperture	6 mm
Basic distance between lens and finger	Uniform between 4 and 6 mm
Focal length of camera	2.753 mm
Width of the joint regions	Uniform between 1.5 and 2 mm
Generating images from same subjects	
Parameter	*Values*
Dilation and erosion width for adjusting joint regions	Uniform between 9 and 10
Dilation and erosion structures	Diamond, disk or square
Range of Perlin noise to adjust the joint regions	Between 0.7 and 1.3
Variation of orientation of Gabor filter ($\Delta\theta_1$ - $\Delta\theta_n$)	Uniform between -0.1 and 0.1
Multiplication factor of the basic density map	Uniform between 0.9 and 1.1
Variation in the depth of the vessels ($\Delta\delta_1$ - $\Delta\delta_n$)	Uniform between -3 and 3
Variation in the depth of the tissues ($\Delta\lambda_1$ - $\Delta\lambda_n$)	Uniform between -0.65 and 0.65
Variation in the distance between lens and finger ($\Delta\zeta_1$ - $\Delta\zeta_n$)	Uniform between -0.5 and 0.5 mm
Thickness of the vessels	Uniform between 2 and 3 mm

shown in figure 26 and the receiver operating characteristics in figure 27. This experiment achieves an equal error rate of 1.59%.

7. Conclusions and Further Work

This technical report has presented the first attempt to model synthetic finger-vein image generation and developed a synthetic finger-vein database of 50,000 images corresponding to 5000 different subjects. Our synthetic vein generation model is based on anatomical characteristics of fingers and incorporates realistic imaging variations introduced in the finger-vein imaging sensors. Our analysis in section 6.2 suggests that the synthesized finger-vein images from the proposed model very closely follow (comparisons using Bessel K form) real finger-vein images acquired using conventional approaches. We also presented matching performance corresponding to 5000 different subjects, using 225,000 genuine and more than 1249 million impostor scores, which indicate significant potential from this modality for the large scale biometrics applications. The finger-vein generator developed from this work is also made publicly available [HK14] for its usage in further research and development for the finger vein biometrics identification.

Despite first promising effort towards synthesizing realistic finger-vein images detailed in this technical report, there are several areas which need further work. In our work we assumed a relative constant illumination between genuine images. During the real finger-vein imaging the variations in the illumination, especially for the same class images, can be much larger. Therefore further work is required to incorporate such significant variations in the imaging. A first start is made, by the analysis of the second generated database, but still more work is needed.

A better look should be taken into the variations between the generated finger-vein patterns. The matching performance indicates a high potential from this modality, but the resulting EER is high, which indicates too large differences between impostor images. More work is needed to reduce the differences between different subjects in the vein pattern generation.

In our work the width of the finger is currently a fixed value for every finger-vein image (2 cm for our experiments). In reality the finger-width is expected to vary for the every subject and every finger. These variations should be accounted in further extension of this work.

Acknowledgment

This work is supported by the research grant from *The Hong Kong Polytechnic University*; grant number PolyU 5011-PPR-12 (K-QZ15) and A-PL85. Fieke Hillerström, has been working as *Research Assistant* in the Department of Computing, The Hong Kong Polytechnic University (February 2014 to June 2014).

June 2014

References

[BGTK06] Alexey N. Bashkatov, Elina A. Genina, Vyacheslav I. Kochubey and Valery V. Tuchin. Optical properties of human cranial bone in the spectral range from 800 to 2000 nm. In *Saratov Full Meeting 2005: Optical Technologies in Biophysics and Medicine VII*. International Society for Optics and Photonics, 2006.

[BK10] A. Buryanov and V. Kotiuk. Proportions of Hand Segments. *Int. J. Morphol*,28(3):755-758, 2010.

[BV99] Volker Blanz and Thomas Vetter. A morphable model for the synthesis of 3D faces. In *Proceedings of the 26th annual conference on Computer graphics and interactive techniques*, pages 187-194. ACM Press, 1999.

[Cap04] Raffaele Cappelli. SFinGe: an approach to synthetic fingerprint generation. In *International Workshop on Biometric Technologies (BT2004)*, pages 147-154, 2004.

[CC+07] Septimiu Crisan, TE Crisan et al. A low cost vein detection system using near infrared radiation. In *Sensors Applications Symposium, 2007. SAS'07. IEEE,* pages 1-6. 2007

[Cup12] NJ. Cuper. Near-infrared vascular imaging in peripheral venous and arterial access. 2012

[KK13] Ajay Kumar and Cyril Kwong, "Towards contactless, low cost and accurate 3D fingerprint identification," *Proc. CVPR 2013*, Portland, pp. 3438-3443, June 2013.

[Gra18] Henry Gray. Anatomy of the human body, 1918.

[GS01] Ulf Grenander and Anuj Srivastava. Probability models for clutter in natural images. *IEEE Transactions on Pattern Analysis and Machine Intelligence*, 23(4):424-429,2001.

[HK14] *Synthetic Finger Vein Image Database Generator*, http://www.comp.polyu.edu.hk/~csajaykr/fvgen.htm, June 2014.

[KP07] Byung Jun Kung and Kang Ryoung Park. Real-time image restoration for iris recognition systems. *IEEE Transactions on Systems, Man, and Cybernetics, Part B: Cybernetics*,37(6):1555-1566, 2007.

[KP09] Ajay Kumar and K. V. Prathyusha. Personal authentication using hand vein triangulation, *Image Processing, IEEE Transactions on*, 38(9): 2127-2136, 2009

[KZ12] Ajay Kumar and Yingbo Zhou. Human identification using finger images. *Image Processing, IEEE Transactions on*, 21(4):2228-2244, 2012.

[LLP09] Eui Chul Lee, Hyeon Chang Lee, and Kang Ryoung Park. Finger vein recognition using minutia-based alignment and local binary pattern-based feature extraction. *International Journal of Imaging Systems and Technology*, 19(3):179-186, 2009.

[Lod99] Guillermo Loda. *Atlas of thumb and finger reconstruction*. Thieme, 1999.

[LP11] Eui Chul Lee and Kang Ryoung Park. Image restoration of skin scattering and optical blurring for finger vein recognition. *Optics and Lasers in Engineering*, 49(7):816-828, 2011.

[MASR14] Mohd Shahrimie, Mohd Asaari, Shahrel A. Suandi and Bakhtiar Affendi Rosdi. Fusion of band limited phase only correlation and width centroid contour distance for finger based biometrics. *Expert Systems with Applications*, 41(7):3367-3382, 2014.

[MNM04] Naoto Miura, Akio Nagasaka and Takafumi Miyatake. Feature extraction of finger-vein patterns based on repeated line tracking and its application to personal identification. *Machine Vision and Applications*, 15(4):194-203, 2004.

[Per] Ken Perlin. Noise and Turbulence. http://mrl.nyu.edu/~perlin/doc/oscar.html

[RFL+05] Adam Runions, Martin Fuhrer, Brendan Lane, Pavol Federl, Anne-Gaëlle Rolland-Lagan and Przemyslaw Prusinkiewicz. Modeling and visualization of leaf venation patterns. In *ACM Transactions on Graphics (TOG)*, volume 24, pages 702-711. ACM, 2005.

[RSS11] Bakthiar Affendi Rosdi, Chai Wuh Shing and Shahrel Azmin Suandi. Finger vein recognition using local line binary pattern. *Sensors*, 11(12):11357-11371, 2011.

[SND+07] A. Sukop, O. Naňka, M. Dušková, M. TVRdek, R. Kufa, O. Měšťák and L. Hauschwitcová. Clinical anatomy of the dorsal venous network in fingers with regards to replantation. *Clinical Anatomy*, 20:77-81, 2007.

[Sri02] Anuj Srivastava. Stochastic models for capturing image variability. *Signal Processing Magazine, IEEE*, 19(5):63-76, 2002.

[Tou80] Godfried T. Toussaint, The relative neighborhood graph of a finite planar set, *Pattern recognition*, 12(4):261-268, 1980.

[TV13] BT Ton and RNJ Veldhuis. A high quality finger vascular pattern dataset collected using a custom designed capturing device. In *Biometrics (ICB), 2013 International Conference on*, pages 1-5. IEEE, 2013.

[WHST08] Zhuoshi Wei, Yufei Han, Zhenan Sun and Tieniu Tan. Palmprint image synthesis: A preliminary study. In *Image Processing, 2008. ICIP 2008. 15th IEEE International Conference on*, pages 285-288, IEEE, 2008.

[XS08] Li Xueyan and Guo Shuxu. The fourth biometric – Vein recognition. *Pattern Recognition Techniques, Technology and Applications*, 626, 2008.

[YLS11] Yilong Yin, Lili Liu and Xiwei Sun. SDUMLA-HMT: a multimodel biometric database. In *Biometric Recognition*, pages 260-268. Springer, 2011.

[YS12] Jinfeng Yang and Yihua Shi. Finger-vein ROI localization and vein ridge enhancement. *Pattern Recognition Letters*, 33(12):1569-1579, 2012.

[YSY10] Jinfeng Yang, Yihua Shi and Junli Yang. Finger-vein recognition based on a bank of Gabor filters. In *Computer Vision-ACCV 2009*, pages 374-383. Springer, 2010.

[YSY12] Jinfeng Yang, Yihua Shi and Jucheng Yang. Finger-Vein image restoration based on a biological optical model. 2012.

[ZLL+13] Congcong Zhang, Xiaomei Li, Zhi Liu, Qijun Zhao, Hui Xu and Fangqi Su. The CFVD reflection-type finger-vein image database with evaluation baseline. In *Biometric Recognition*, pages 282-287. Springer 2013.

[ZSC07] Jinyu Zuo, Natalia A. Schmid and Xiaohan Chen. On generation and analysis of synthetic iris images. *Information Forensics and Security, IEEE Transactions on*, 2(1):77-90, 2007.